Navier-Stokes Calculations for Unsteady Three-Dimensional Vortical Flows in Unbounded Domains

James P. Chamberlain* and C. H. Liu*
NASA Langley Research Center, Hampton, Virginia

Finite difference Navier-Stokes calculations for unsteady, three-dimensional, incompressible, viscous flows induced by initial vorticity distributions are presented and discussed herein. The initial vorticity distributions are assumed to be embedded in a flowfield of infinite extent that is quiescent at infinity. These vorticity distributions are typical of vortex rings and other closed vortical tubes or structures. Such structures are important elements in fluid flows such as jets, atmospheric convection, and the far-field wakes of aircraft, and studies of their interaction may aid in an understanding of complex fluid flows. The calculations employ a method recently proposed by Ting to approximate the infinite domain boundary value problem with a finite boundary computational domain. This method is shown to yield accurate three-dimensional results for reasonable expenditures of computer time. Because of the efficiency of the boundary condition technique and the resulting Navier-Stokes code, a 16-bit minicomputer with virtual memory was capable of performing the calculations for the unsteady motion of two obliquely colliding vortex rings. The results of these calculations are presented in this paper.

Introduction

VORTEX-dominated flows in unbounded fluid domains comprise an important class of problems in fluid dynamics. Some examples of such flows are the phenomena of atmospheric turbulence and convection,[1] the flowfields in the vicinity of free jets,[2] and the far-field wakes of aircraft.[3,4] These flows are often very complex and are characterized by the time-dependent, three-dimensional motion and deformation of vortex tubes or structures. The interaction and decay of these vortex structures in time is often dominated or at least influenced by the effects of viscosity, so that solutions of many free vortex flow problems must, in some way, account for viscous effects. In addition, a numerical solution to a free vortex flow problem must use a finite computational domain to simulate or approximate the unbounded domain fluid flow.

One method of approximating an infinite domain fluid flow problem numerically is to specify the infinity boundary conditions along the finite boundary of a computational domain. For example, if the velocity is assumed to vanish at infinity, then an approximate numerical boundary condition would set the velocity to zero at the boundary of the finite computational domain. However, this approach generally requires a large computational domain to reduce the error introduced at the boundary and, therefore, a large percentage of the total computing time may be spent calculating the flow outside the primary region of interest.

A better method of specifying the conditions on the finite domain boundary is to estimate the behavior of the solution at the boundary based on integral quantities of the solution in the domain interior. This type of boundary condition method generally allows the size of the computational domain to be reduced without increasing the error introduced at the boundary. This method of boundary condition specification was used by Bilanin et al.[5] in 1977 to compute the two-dimensional incompressible rollup of aircraft wakes, and more recently by Weston and Liu.[6] Weston and Liu also used the integral quantities in a manner that allowed the solution accuracy to be monitored in time. Variations of the method were also employed by Liu and Ting[7] and Liu et al.[8] to calculate the motion of axisymmetric vortex rings and the vortex wake rollup of a rotor in hover, respectively. A technique for using this boundary condition method to calculate the three-dimensional motion and interaction of closed vortex tubes was recently proposed by Ting,[9] and this technique is incorporated in the code presented in this paper.

Finite difference Navier-Stokes calculations for unsteady, three-dimensional, incompressible, vortex-dominated flows are presented and discussed in this paper. The three-dimensional problem formulation is presented in the first section of the paper, and is followed by a discussion of the approximate boundary condition technique. Subsequent sections of the paper contain a description of the computer code used to calculate the fluid flow, computed results that demonstrate the accuracy and efficiency of the boundary condition technique, and results from the computer code for the unsteady motion of two obliquely colliding vortex rings.

Problem Formulation

The governing equations for viscous incompressible flow are

$$\nabla \cdot V = 0 \tag{1}$$

$$\frac{\partial V}{\partial t} = -(V \cdot \nabla)V - \frac{1}{\rho}\nabla p + \nu \nabla^2 V \tag{2}$$

where V is the fluid velocity and ρ and ν the constant fluid density and kinematic viscosity, respectively. The appropriate initial and boundary conditions for Eqs. (1) and (2) are

$$V(x,0) = V_0(x) \tag{3}$$

$$|V(x,t)| \to 0 \text{ and } p(x,t) \to p_\infty \text{ as } |x| \to \infty \tag{4}$$

where V_0 and p_∞ are specified. The initial boundary value problem described by Eqs. (1-4) can be formulated also in terms of the vorticity and vector velocity potential variables, and this approach is used here.

The vorticity Ω is defined as the curl of the velocity,

$$\Omega = \nabla \times V \tag{5}$$

Received Dec. 19, 1983; presented as Paper 84-0418 at the AIAA 22nd Aerospace Sciences Meeting, Reno, Nev., Jan. 9-12, 1984; revision received July 17, 1984. This paper is declared a work of the U.S. Government and therefore is in the public domain.

*Research Scientist, Analytical Methods Branch, Low-Speed Aerodynamics Division. Member AIAA.

and since the velocity field is divergence free, it may be expressed as the curl of a vector velocity potential A,

$$V = \nabla \times A \tag{6a}$$

The curl of any gradient vector is zero, so A is indeterminate to the extent of the gradient of a scalar function of position and time.[10] The divergence of A can thus be specified as

$$\nabla \cdot A = 0 \tag{6b}$$

so that, by vector identity, the vector potential and vorticity are related by the vector Poisson equation

$$\nabla^2 A = -\Omega \tag{7}$$

The transport equation for Ω can be obtained by taking the curl of Eq. (2), which yields

$$\frac{\partial \Omega}{\partial t} = -(V \cdot \nabla)\Omega + (\Omega \cdot \nabla)V + \nu \nabla^2 \Omega \tag{8}$$

In the numerical computations the conservation form of Eq. (8) is used, which can be expressed as

$$\frac{\partial \Omega}{\partial t} = \nabla \times (V \times \Omega) + \nu \nabla^2 \Omega \tag{9}$$

If the fluid velocity is zero at infinity, then the solution of Eq. (7) is the Poisson integral,

$$A(x,t) = \frac{1}{4\pi} \int_{-\infty}^{\infty} \int \int \frac{\Omega(x',t)}{|x - x'|} dx' \tag{10}$$

where x' is the variable of integration and $dx' = dx_1' dx_2' dx_3'$. Equation (10) can be combined with Eqs. (6-9) to form a single integrodifferential equation in Ω; the appropriate initial and boundary conditions are then

$$\Omega(x,0) = \Omega_0(x); \quad \nabla \cdot \Omega_0 = 0 \tag{11a}$$

$$\Omega(x,t) \to 0 \text{ as } |x| \to \infty \tag{11b}$$

where Ω_0 is a specified initial vorticity distribution. For concentrated distributions of vorticity Ω will approach zero much faster than V as $|x| \to \infty$; thus, if Ω and A are used as primary variables rather than V and p, then a smaller computational domain can be used without increasing the error due to the finite domain boundary. For the calculations to be presented herein Ω and A are used as primary variables, and the initial vorticity distributions are assumed to decay at least exponentially as $|x| \to \infty$. The computational error due to the specification of boundary condition (11b) on the finite boundary $|x| = R$ will then be $\mathcal{O}(e^{-R})$. This finite boundary error is much smaller than the boundary error incurred by the primitive variable boundary condition $|V| = 0$, which is generally $\mathcal{O}(R^{-3})$. An additional source of error will arise due to the evaluation of the Poisson integral over only the computational space, but this error is of the same order as the error due to the finite boundary specification of Ω, or $\mathcal{O}(e^{-R})$.

The integrodifferential equation formed by Eqs. (6), (9), and (10) can be solved numerically to yield $\Omega(x,t)$; this approach has been used by several researchers[11,12] for two-dimensional problems. However, this approach is very time consuming numerically, since the Poisson integral must be evaluated at each grid point to obtain A. For a three-dimensional computational domain containing N^3 grid points, the determination of A at all grid points using the Poisson integral would require $\mathcal{O}(N^6)$ operations. For dense grids the integrodifferential equation approach becomes prohibitively expensive.

Boundary Conditions

Efficient numerical schemes are available[13] for the solution of the Poisson equation (7) using $\mathcal{O}(N^3 \log N)$ operations; these schemes can be used to obtain A more efficiently than by using the Poisson integral. However, in order to solve Eq. (7), A must be specified on the finite computational boundary, and if the Poisson integral is used to obtain these boundary values then the total number of operations to obtain A at all points becomes $\mathcal{O}(N^5)$. The value of A at the boundary could be specified so that $|V| = 0$ on the boundary, or A could be set to some constant value (which is equivalent to stating that the normal velocity at the boundary is zero), but these approximate boundary conditions are generally accurate only to $\mathcal{O}(R^{-3})$ and, thus, will require large computational domains.

A more accurate method for obtaining the required boundary values of A, while avoiding the expense of computing the Poisson integral, is to approximate the far-field behavior of the integral. Such a method has been proposed by Ting[9]; this method is described in the remainder of this section. The method has the additional advantage of providing integral checks of the global solution accuracy.

If the vorticity decays at least exponentially in $|x|$, then the denominator of the Poisson integral can be expanded and A can be expressed as a power series in $1/r$,

$$A(x,t) = \frac{1}{4\pi} \sum_{n=0}^{m} A^{(n)}(\hat{r},t) r^{-n-1} + \mathcal{O}(r^{-m-2}) \tag{12a}$$

$$A^{(n)}(\hat{r},t) = \int_{-\infty}^{\infty} \int \int \Omega(x',t)(r')^n P_n(\hat{r} \cdot \hat{r}') dx' \tag{12b}$$

where $\hat{r}$ and $\hat{r}'$ are unit vectors in the directions of x and x', respectively, P_n is a Legendre polynomial, and r and r' the magnitudes of x and x', respectively. Ting points out that $r^n A^{(n)}$ is a homogeneous polynomial of degree n in the Cartesian components x_i, and that its coefficients are the nth moments of vorticity. This fact allows Eq. (12b) to be rearranged so that the volume integrals required to determine $A^{(n)}(\hat{r},t)$ are independent of $\hat{r}$. The first three terms of Eqs. (12) are

$$A^{(0)} = \sum_{i=1}^{3} \langle \omega_i \rangle \hat{e}_i \tag{13}$$

$$A^{(1)} = \sum_{i=1}^{3} \sum_{j=1}^{3} \langle x_j \omega_i \rangle \lambda_j \hat{e}_i \tag{14}$$

$$A^{(2)} = \sum_{i=1}^{3} \sum_{j=1}^{3} \sum_{k=1}^{3} \langle x_j x_k \omega_i \rangle \frac{1}{2}(3\lambda_j \lambda_k - \delta_{jk}) \hat{e}_i \tag{15}$$

where λ_i are the components of $\hat{r}_i$, ω_i the components of Ω, $\hat{e}_i$ the unit vectors parallel to the Cartesian coordinate axes, and $\langle\ \rangle$ indicate volume integration over all space.

Equations (13), (14) and (15) contain three, nine, and eighteen volume integrations, respectively, but not all of these integrals need to be evaluated. Integral invariants of the vorticity and consistency conditions based on the divergence-free character of Ω can be applied to reduce the number of independent integral quantities required for the evaluation of Eqs. (13-15). Specifically, it can be shown[14] from the divergence-free condition and the far-field behavior of Ω that the nth coaxial moment along an axis parallel to a vector B will vanish,

$$\int_{-\infty}^{\infty} \int \int [B \cdot x']^n B \cdot \Omega(x',t) dx' = 0 \tag{16}$$

Equation (16) can be applied for $n = 0$, 1, and 2 to show that 1) all three integral quantities in Eq. (13) are zero, i.e., $\langle \Omega \rangle = 0$ for all time, 2) only three of nine integrals in Eq.

(14) are independent and nonzero, and 3) only eight of eighteen integrals in Eq. (15) are independent and nonzero. In addition, integral invariants of the vorticity[15,16] based on conservation of linear and angular momentum can be applied to show that all three of the independent integrals in Eq. (14) and three of eight integrals in Eq. (15) are time invariant. These six time-invariant integrals can thus be evaluated for the initial vorticity distribution Ω_0, and at any later instant in time the five remaining integrals can be evaluated to yield the quantities necessary to compute $A^{(0)}$, $A^{(1)}$, and $A^{(2)}$. The six time-invariant integrals can also be numerically re-evaluated for $t>0$ to monitor the accuracy of the computed results as the calculations proceed in time.

Equations (13-15), for the first three coefficients of Eqs. (12), can be rewritten after the simplifications discussed above.

$$A^{(0)} = 0 \tag{17}$$

$$A^{(1)}(\hat{r}) = \sum_{k=1}^{3} C_k(\lambda_i \hat{e}_j - \lambda_j \hat{e}_i) \tag{18}$$

$$A^{(2)}(\hat{r},t) = \frac{3}{4}\sum_{k=1}^{3} D_k[(\lambda_i^2+\lambda_j^2-\tfrac{2}{3})\hat{e}_k - \lambda_k(\lambda_i\hat{e}_i+\lambda_j\hat{e}_j)] + \frac{3}{4}\sum_{k=1}^{3} G_k(t)[(\lambda_i^2-\lambda_j^2)\hat{e}_k - \lambda_k(\lambda_i\hat{e}_i-\lambda_j\hat{e}_j)] + \sum_{k=1}^{3} H_k(t)\lambda_i\lambda_j\hat{e}_k \tag{19}$$

where

$$C_k = \langle x_i\omega_j \rangle \tag{20}$$

$$D_k = \langle r^2\omega_k \rangle \tag{21}$$

are time invariant, and

$$G_k(t) = \langle (x_i^2 - x_j^2)\omega_k \rangle \tag{22}$$

$$H_k(t) = \langle 2x_ix_j\omega_k - x_ix_k\omega_j - x_kx_j\omega_i \rangle \tag{23}$$

vary with time [only two of the three integrals in Eq. (23) are independent, since $H_1+H_2+H_3=0$]. The indices in Eqs. (18-20), (22) and (23) are chosen so that $i\neq j\neq k$ and $i<j$. Equations (17-19) can be substituted into Eqs. (12) to yield boundary values of A to terms of $\mathcal{O}(R^{-3})$. The error due to the boundary values of A will therefore be $\mathcal{O}(R^{-4})$, and the velocity error will be $\mathcal{O}(R^{-5})$. While it may be possible to improve the accuracy of the boundary values of A by including terms in Eqs. (12) involving higher moments of the vorticity, these terms would probably be difficult to evaluate accurately since small numerical errors in the far-field vorticity distribution would be amplified in the higher moment evaluations.

One further relationship can be derived which expresses the rate of decay of total kinetic energy,

$$\langle V\cdot V \rangle = \langle A\cdot\Omega \rangle = \langle A\cdot\Omega_0 \rangle_{t=0} - 2\nu\int_0^t \langle \Omega\cdot\Omega \rangle d\tau \tag{24}$$

This decay law is obtained by taking the scalar product of the momentum equation and the velocity, integrating the result over all space, and applying the divergence theorem and various vector identities. The decay law can be numerically integrated in time either during or after the Navier-Stokes calculations, and can be used as a global check of numerical diffusion effects and total kinetic energy dissipation. The deviations of the numerical results from the decay law and the integral invariants thus can be used to estimate the error of the numerical solutions.

Computer Code

A computer code has been developed to evaluate the system of Eqs. (6-9) using the boundary conditions discussed in the previous section. The code employs a uniform Cartesian finite difference computational domain in three dimensions and is coded in the FORTRAN 77 programming language. The program was initially developed on a 16-bit Hewlett-Packard 1000F minicomputer for two reasons. First, development of the code on a minicomputer allowed for rapid turnaround time during the edit, compile, and debug stages, and allowed for a reasonable amount of numerical experimentation without incurring the expense of mainframe computing. Second, the initial operation of the code on a minicomputer ensured that any advantages of the algorithm would be transportable, i.e., supercomputer capabilities such as vector processing or extreme amounts of core memory would not be required for performance of the algorithm. All of the results presented in this paper were obtained with the minicomputer, although the code has been moved to a Control Data Cyber 203 computer for higher resolution solutions on more dense grids. For a grid with 33 points in each direction the code requires approximately 14 min/time step on the minicomputer; each time step requires approximately 11 s to execute in scalar mode on the Cyber 203.

The basic algorithm performed by the program is shown in Fig. 1 along with the relative computer times required for the primary computational steps. These steps are described briefly as follows.

1) The eleven volume integrals described by Eqs. (20-23) are evaluated using Simpson integration over the computa-

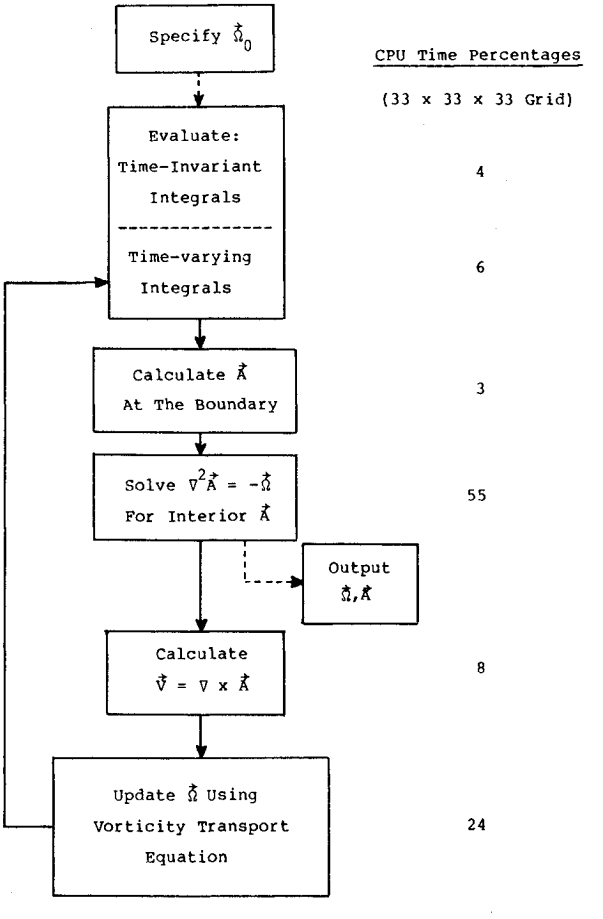

Fig. 1 Logical flowchart of Navier-Stokes code.

tional domain. The five time-varying integrals, Eqs. (22) and (23), are evaluated at each time step, while the six time-invariant integrals are evaluated initially and then only periodically to monitor the accuracy of the solution.

2) The results from step 1 are substituted into Eqs. (18) and (19) and the resulting coefficients $A^{(1)}$ and $A^{(2)}$ are used with Eqs. (12) to determine values of A at the boundary.

3) A fast Poisson solver is used to determine the values of A in the interior of the computational domain. The solver currently in use is a direct method developed by the National Center for Atmospheric Research (NCAR).[13] The method uses a finite difference formulation and is second-order accurate in the spatial directions.

4) The velocity field is obtained using second-order centered differences to obtain the curl of A. The velocity values are written over the vector potential values to minimize the required computer storage.

5) The vorticity field is advanced in time using a finite difference representation of the vorticity transport equation (9). The program currently uses the Dufort-Frankel method to solve for the vorticity transport equation; this explicit method is accurate to $\mathcal{O}[(\Delta t)^2, (\Delta x_i)^2, \nu(\Delta t/\Delta x_i)^2; i=1,2,3]$. Explicit methods to solve the vorticity transport equation appear to be more appropriate than implicit methods in this case for two reasons. First, in order to attain a time-accurate solution to the unsteady flow problem relatively small time steps must be taken, and these small time steps tend to negate the efficiency of the implicit methods. Second, three-dimensional finite difference grids tend to be coarser than grids in fewer dimensions, so the explicit stability limitation on the time step size is not significantly smaller than the step size required for time accuracy.

Steps 1-5 are repeatedly applied to advance the finite difference solution in time.

Boundary Condition Accuracy

The accuracy and efficiency of two approximate vector potential boundary condition methods were evaluated for a specified vorticity distribution. These two methods were the truncated series method discussed above and a method that enforces zero-normal velocity at the boundary; the zero-normal velocity boundary condition was enforced by setting $|A|$ to zero at the boundary. The accuracies of the methods were determined by comparing the two approximate boundary condition solutions with a solution that used Poisson integral evaluations to generate the boundary conditions. Two types of comparisons with the Poisson boundary condition method were made. First, the differences between the Poisson integral boundary values and the approximate boundary values were measured to indicate the errors of the approximate boundary methods. Second, the interior solutions were compared with the Poisson boundary condition interior solution to determine the global solution error caused by the boundary condition errors. The efficiencies of the methods were evaluated by comparing the computer execution times required to calculate the vector potential boundary values and solution. Results of the comparisons of the two approximate boundary methods with the Poisson boundary method for a specified vorticity distribution are discussed below.

The vorticity distribution chosen for the boundary condition checks is illustrated in Fig. 2. This distribution represents two vortex rings with equal strengths, radii, and filament diameters whose axes of symmetry lie in the x-y plane and cross each other at an angle of 45 deg. The angle formed by the two axes of symmetry is bisected by the x axis, and the centers of the rings lie on the y axis at ± 1.5 units, where a unit of length represents the toroidal radius of each ring. The form of the vorticity distribution through the ring core is Gaussian, and the effective cross-sectional radius of the rings (the radius at which the vorticity magnitude has fallen to $1/e$ of the maximum vorticity magnitude) is 0.5. The computational domain is a cube centered about the origin with edges of length 8. This domain size is the practical minimum cubical size that will still enclose both vortical rings, and thus represents a "worst-case" test condition for the two vector potential boundary condition methods under consideration.

Table 1 shows interior and boundary value normalized errors for the series method and zero-normal velocity boundary condition solutions. These interior and boundary value errors are expressed as rms errors over the interior and boundary grid points, respectively, and are normalized by the maximum magnitude of A in the interior of the Poisson integral boundary condition solution. Table 1 also shows the execution times required to compute the boundary and interior values of A for each method. The Poisson integral boundary condition case was computed only for the domain with sides of length 8 and 17 points along a domain edge,

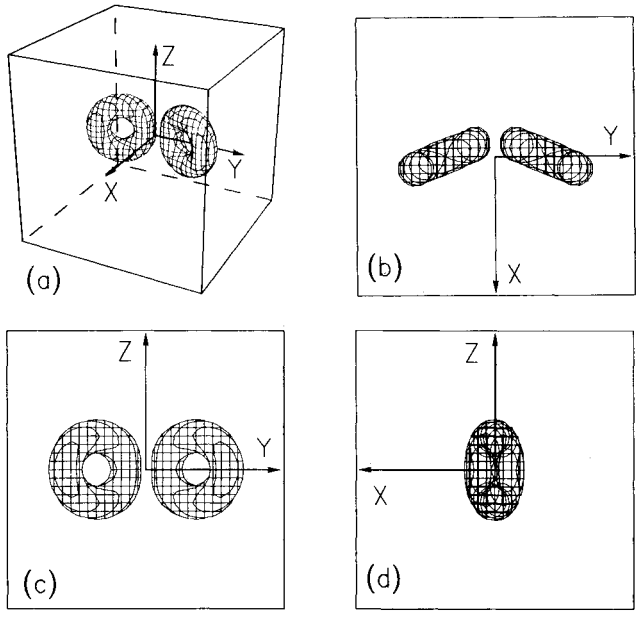

Fig. 2 Initial vorticity distribution isosurface sketch, two obliquely colliding vortex rings. a) perspective view, b) top view, c) front view, d) right-side view.

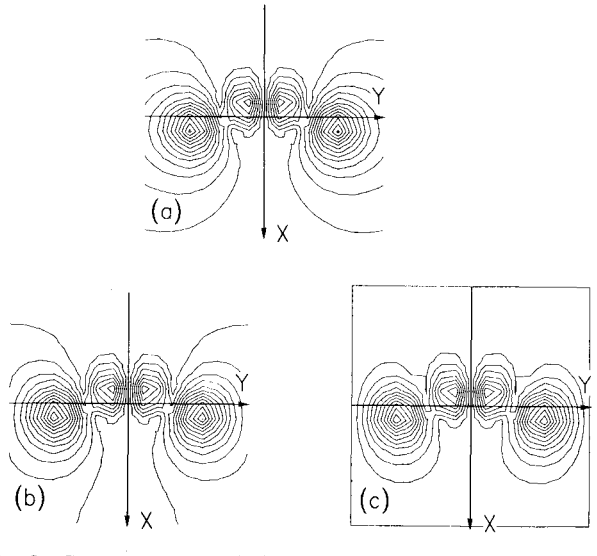

Fig. 3 Contour plots of $|A|$ in x-y plane for a) Poisson integral boundary conditions, b) series method boundary conditions, and c) $|A|=0$ boundary conditions.

whereas the series method and zero-normal velocity cases were run for the two larger domains as well. The edge lengths and number of grid points in the two larger domains are adjusted so that the grid spacing is identical for all three domains. The normalized errors obtained for the two larger domains were obtained by considering only the region common to the smallest domain as the solution space. Therefore, results from the two larger domains are useful in determining the required domain size for each method to obtain an accurate solution in the region of interest.

The error figures shown in Table 1 indicate that the series method for obtaining boundary data yields more accurate results than the zero-normal velocity method for a given domain size. In fact, for the test case chosen, the interior solution for A obtained using series method boundary data is better than the zero-normal velocity solution obtained on a domain nearly twice as large. In this case, the series method solution requires less than one-sixth the time required for the zero-normal velocity solution of equivalent accuracy. For equivalent grids, the series method takes slightly more execution time than the zero-normal velocity method, but this relative time difference diminishes as the grid density increases, since the ratio of boundary to interior points decreases.

Figure 3 shows contour plots of the magnitude of A in the x-y plane of the smallest domain for each of the three boundary condition methods. The contour lines represent lines of constant vector potential magnitude and are equally spaced from a value of zero to a value of 0.98 times the maximum magnitude of A in the Poisson boundary condition solution. These lines can be thought to be the intersection of stream surfaces of the solution with the x-y plane. It is evident from Fig. 3 that the finite solution domain affects both the series method and zero-normal velocity method solutions, although the series solution is not affected to nearly as great an extent. For slightly larger domains the series method solution closely approximates the Poisson method solution, whereas the global character of the zero-normal velocity solution is altered by the closed boundary.

The execution times shown in Table 1 indicate that, for the smallest domain, the Poisson integral boundary condition method requires about 150 times more computer time to compute A than the series method. Since the number of required operations for the Poisson method rises as the fifth power of the number of grid points along an edge, this method would require nearly 6000 times more execution time than the series method for a grid of 100 points on each edge. Thus, even though the Poisson integral boundary condition method is based on the exact solution for the boundary data, the method is not practical for numerical computations.

Sample Results

The oblique collision and interaction of two vortex rings was chosen as a test case to demonstrate the code, and the vorticity distribution described in the previous section (see Fig. 2) was used as the initial condition. This test case was chosen for two reasons. First, qualitative experimental observations of colliding vortex rings are available[17,18] for comparison with the code results. Second, the experimental observations[17-19] indicate that both merging and three-dimensional deformation of the rings occur, so that both viscous and convective forces should be important in this flow problem.

The primary objective of the test case was to verify qualitative agreement with experimental observations rather than to compute a high-accuracy solution to a particular

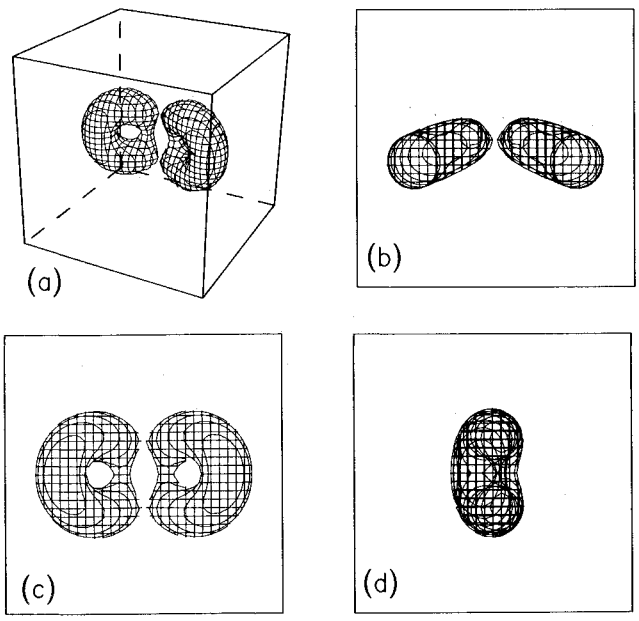

Fig. 4 Initial vector potential isosurface sketch, a) perspective view, b) top view, c) front view, d) right side view.

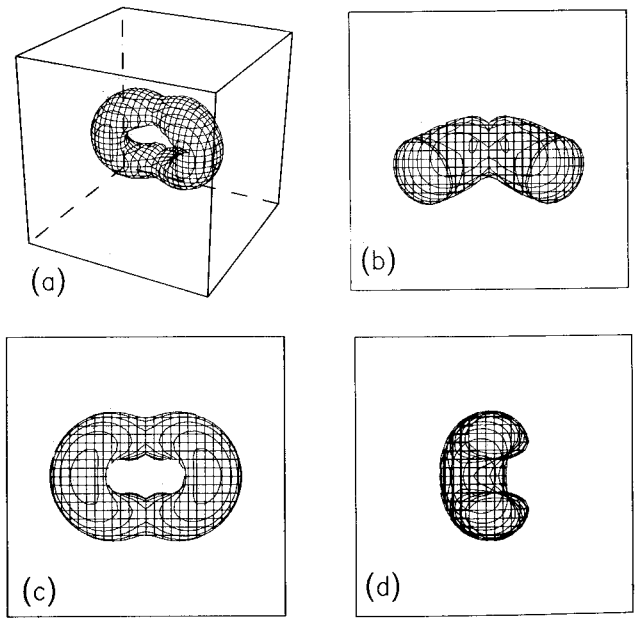

Fig. 5 Vector potential isosurface sketch at $t\,|\Omega_0|_{max} = 10.4$.

Table 1 Effect of computational boundary on error and cost

Cubical domain edge length	No. of points on grid edge	rms vector potential errors, %		Execution time, s		
		Series	$\|A\| = 0$	Series	$\|A\| = 0$	Poisson
8	17	1.63	7.51	57.8	42.5	8695.0
12	25	0.659	2.48	226.0	182.0	—
14	29	0.620	1.67	431.0	363.0	—

flow problem. Therefore, the grid density was limited to 33 points along each edge of a cubical solution domain. The length of each domain side was 8 ring radii, which produced a grid spacing intended to yield good resolution of the interior solution while maintaining acceptable finite boundary errors. The domain was allowed to translate with the initial vorticity-weighted average velocity of the rings, which tended to keep the vorticity centered within the domain. The Reynolds number of the computed time-dependent solution was 785, where the Reynolds number was defined as the ring circulation divided by the kinematic viscosity.

Figures 4-9 represent the consecutive advancement of the calculated solution in time. The orientation of the axes in these figures is the same as in Fig. 2. Part a of each figure contains a perspective sketch of the 50% vector potential magnitude isosurface at a particular instant in time; the sketch of the cube represents the solution domain boundary. The vector potential magnitude isosurface approximates a stream surface and thus probably approximates the form of entrained smoke used to experimentally visualize vortex rings. The initial 50% magnitude isosurface contains most of the vorticity in the domain and, therefore, should be a good representation of the vortex rings. Parts b, c, and d of each figure contain top, front, and right side views of the isosurface, respectively. A simple hidden line algorithm was developed to generate the isosurface sketches and requires a brief explanation to avoid misinterpretation of the sketches. A section of the surface is considered hidden if the dot product of the viewing direction and the solution gradient at the surface are negative. This algorithm is fast and will draw only isosurface sections facing the viewer, but it cannot determine whether a surface facing the viewer is behind another surface. Therefore, any overlapping sections of the isosurfaces in Figs. 4-9 will both be drawn.

Figure 4 shows the initial vector potential magnitude isosurface for the two rings; the rings are moving in the positive x direction and toward each other. The rings thus appear to move down and inward in the top view (b) and toward the viewer in the front view (c). The rings are moving to the left in the right side view (d). The distortion of the two surfaces in the center is due to the mutual influence of the two rings in this region; the velocity influences of the rings are additive in this region and the maximum field velocity occurs here.

Figure 5-8 show the subsequent merging of the two rings into a single distorted oblong ring, and the switching of roles of the major and minor axes of the ring. This behavior is in good qualitative agreement with experimental flow visualization.[17-19] The average error of the time-invariant integral quantities is less than 1% for the results in Figs. 5-8, and this low error level provides a degree of confidence in the calculated results. References 17-19 also indicate that, in some cases, the single ring formed after the collision will split again into two rings, except that the line joining the centers of the two new rings is perpendicular to the line joining the original ring centers. The beginning of this splitting behavior may be occurring in Fig. 9, but the results shown in Fig. 9 are suspect for several reasons. The deformation and diffusion of vorticity have caused the solution to come very close to the side of the computational domain at the time shown in Fig. 9. In addition, the merging of the two rings into one and the enlargement of the effective toroidal and cross-sectional radii have caused the resultant ring to slow

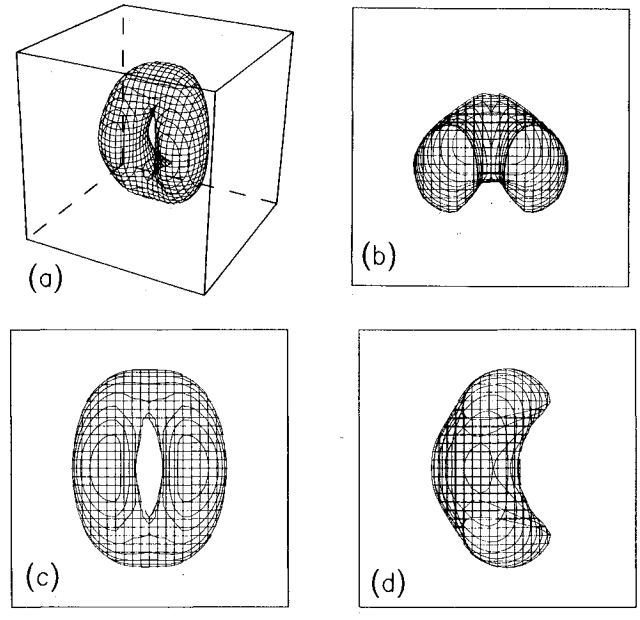

Fig. 7 Vector potential isosurface sketch at $t\,|\Omega_0|_{\max} = 40.9$.

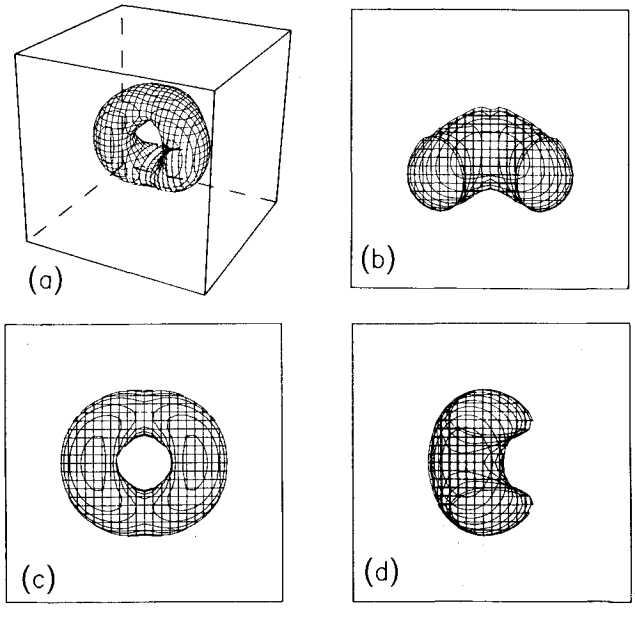

Fig. 6 Vector potential isosurface sketch at $t\,|\Omega_0|_{\max} = 20.2$.

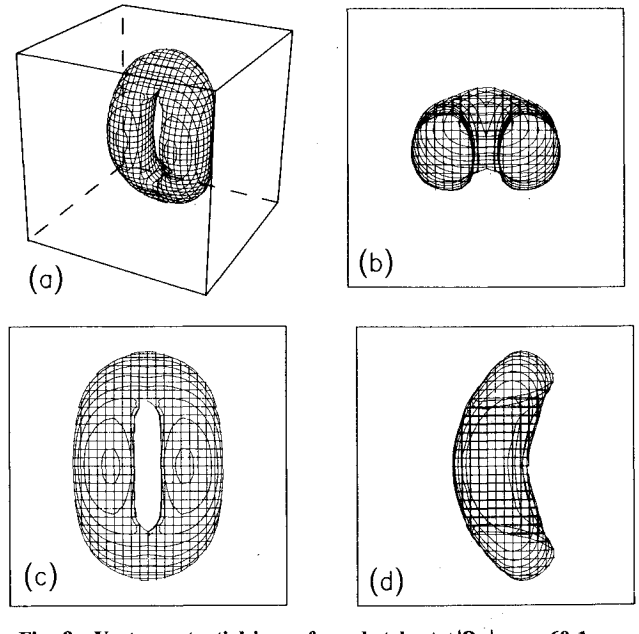

Fig. 8 Vector potential isosurface sketch at $t\,|\Omega_0|_{\max} = 60.1$.

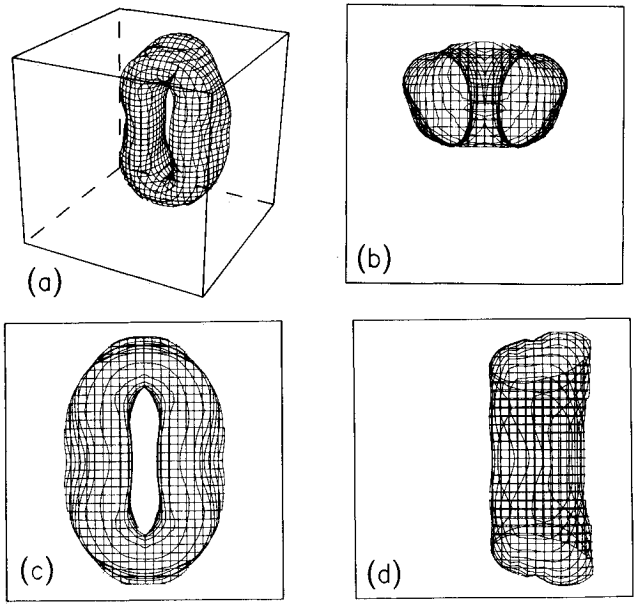

Fig. 9 Vector potential isosurface sketch at $t|\Omega_0|_{max} = 96.3$.

down (due to conservation of linear momentum), so that the computational domain has begun to overrun the solution. The proximity of the solution to the boundary affects the solution accuracy, and the effect on the accuracy is indicated by the time-invariant integral quantities. For Fig. 9, the error in the quantities is about 6%, and the boundary error is also visually apparent near the ring major axis.

Conclusions

An unsteady, three-dimensional, incompressible, Navier-Stokes code for vortex flows in unbounded domains has been developed, and sample results from the code have been presented in this paper. The code uses an approximate boundary condition procedure to simulate the infinite fluid domain. This procedure has proven to be both accurate and efficient. Relevant time-invariant integrals of the vorticity distribution and a decay law for kinetic energy have also been shown to be useful in the numerical calculation of flowfields. The deviations of the numerical results from these integral relationships can be used to measure the overall effects of the computational domain size and numerical algorithm on the accuracy of the solution. Good qualitative agreement between the calculated results and the available experimental data was demonstrated for the oblique collision and merging of two vortex rings. The application of this code to other problems involving closed vortical structures is straightforward and may provide some enlightening results.

References

[1]Turner, J. S., "Buoyant Plumes and Thermals," *Annual Reviews of Fluid Mechanics*, Vol. 1, 1969, pp. 29-44.

[2]Crow, S. C. and Champagne, F. H., "Orderly Structure in Jet Turbulence," *Journal of Fluid Mechanics*, Vol. 48, 1974, pp. 547-591.

[3]Van Dyke, M., *An Album of Fluid Motion*, The Parabolic Press, Stanford, Calif., 1982.

[4]Cornish, J. J. III, "Vortex Flows," Lockheed-Georgia Co., Marietta, Ga., 1982.

[5]Bilanin, A. J., Teske, M. E., Donaldson, C. duP., and Williamson, G. G., "Vortex Interactions and Decay in Aircraft Wakes," NASA CR-2870, Sept. 1977.

[6]Weston, R. P. and Liu, C. H., "Approximate Boundary Condition Procedure for the Two-Dimensional Numerical Solution of Vortex Wakes," AIAA Paper 82-0951, June 1982.

[7]Liu, C. H. and Ting, L., "Numerical Solution of Viscous Flow in Unbounded Fluid," *Eighth International Conference on Numerical Methods in Fluid Dynamics, Proceedings, Lecture Notes in Physics*, Vol. 170, Springer-Verlag, Germany, 1982, pp. 357-363.

[8]Liu, C. H., Thomas, J. L., and Tung, C., "Navier-Stokes Calculations for the Vortex Wake of a Rotor in Hover," AIAA Paper 83-1676, July 1983.

[9]Ting, L., "On the Application of the Integral Invariants and Decay Laws of Vorticity Distributions," *Journal of Fluid Mechanics*, Vol. 127, Feb. 1983, pp. 497-506.

[10]Karamcheti, K., *Principles of Ideal Fluid Aerodynamics*, Robert E. Krieger Publishing Co., Malabar, Fla., 1966.

[11]Wu, J. C. and Thompson, J. F., "Numerical Solutions of Time-Dependent Incompressible Navier-Stokes Equations Using an Integro-Differential Formulation," *Computers & Fluids*, Vol. 1, 1973, pp. 197-215.

[12]Lo, R.K.C. and Ting, L., "Studies of the Merging of Vortices," *The Physics of Fluids*, Vol. 19, No. 6, 1976, pp. 912-913.

[13]Swarztrauber, P. N. and Sweet, R. A., "ALGORITHM 541, Efficient FORTRAN Subprograms for the Solution of Separable Elliptic Partial Differential Equations [D3]," *ACM Transactions on Mathematical Software*, Vol. 5, No. 3, Sept. 1979, pp. 352-364.

[14]Truesdell, C., *The Kinematics of Vorticity*, Indiana University Press, Bloomington, Ind., 1954.

[15]Moreau, J.-J., "Sur deux theoremes generaux de la dynamique d'un milieu incompressible illimite," *Comptes Rendus de l'Academie des Sciences*, Vol. 226, 1948, pp. 1420-1422.

[16]Moreau, J.-J., "Sur la dynamique d'un ecoulement rotationnel," *Comptes Rendus de l'Academie des Sciences*, Paris 229, 1949, pp. 100-102.

[17]Fohl, T. and Turner, J. S., "Colliding Vortex Rings," *The Physics of Fluids*, Vol. 18, April 1975, pp. 433-436.

[18]Oshima, Y. and Asaka, S., "Interaction of Two Vortex Rings Moving Side by Side," *Natural Science Report*, Vol. 26, No. 1, 1975, pp. 31-37.

[19]Oshima, Y. and Osaka, S., "Interaction of Two Vortex Rings Along Parallel Axes in Air," *Journal of the Physical Society of Japan*, Vol. 42, No. 2, Feb. 1977, pp. 708-713.